

# Carbon Nanotubes Potentialities in Directional Dark Matter Searches

LM Capparelli\*, G Cavoto<sup>¶</sup>, D Mazzilli\* and AD Polosa\*,<sup>¶</sup>

*\*Dipartimento di Fisica, Sapienza Università di Roma, Piazzale Aldo Moro 2, I-00185 Roma, Italy*

*<sup>¶</sup>INFN Sezione di Roma, Piazzale Aldo Moro 2, I-00185 Roma, Italy*

Saturday 7<sup>th</sup> December, 2024

## Abstract

We propose a new solution to the problem of dark matter directional detection based on large parallel arrays of carbon nanotubes. The phenomenon of ion channeling in single wall nanotubes is simulated to calculate the expected number of recoiling carbon ions, due to the hypothetical scattering with dark matter particles, subsequently being driven along their longitudinal extension. As shown by explicit calculation, the relative orientation of the carbon nanotube array with respect to the direction of motion of the Sun has an appreciable effect on the channeling probability of the struck ion and this provides the required detector anisotropic response.

PACS: 95.35.+d, 61.48.De

# 1 Introduction

The most striking evidence of the weakly interacting massive particle (WIMP) nature of dark matter reported so far comes from the annual modulation in nuclear recoil rates observed by the DAMA/LIBRA experiment at INFN Gran Sasso, Italy [1].

Unfortunately, their impressive results, briefly reviewed also in this paper, have never been significantly confirmed by any other direct dark matter search experiment. Moreover, some experimental results, obtained with different techniques, are interpreted to be in contradiction with the DAMA/LIBRA ones [2].

Reproducing and understanding the annual modulation effect is an urgent and overdue effort high in the task list of dark matter experimental physics. However it is commonly believed that it would be preferable to use the *same* detection technology (based on NaI crystals) in similar shielding and radiopurity conditions, but in some different laboratory and with independent analysis techniques.

WIMPs might be the constituents of a diffuse dark matter halo we are traveling through with a velocity that changes during the Earth's revolution around the Sun. The rare interactions of WIMPs with detector nuclei (sodium or iodine nuclei, or even electrons [3], as in the case of DAMA/LIBRA) might cause the latter to recoil out of their crystal sites releasing energy through ionization. The effect of the variable relative velocity of WIMPs at different times of the year might eventually be detected, yet nothing can be concluded, with the apparatuses being used, about their (average) direction, namely the WIMP wind direction.

In other words, dark matter direct search experiments are presently unable to discern nuclear recoil directions although there are several attempts and proposals to solve this problem, such as the one by the DRIFT collaboration, see *e.g.* [4].

In this paper we address the issue of directional detection of dark matter with a new approach: channeling within single wall carbon nanotubes (CNT). The unit component of the detector we want to study is a CNT closed at one end and open at the other. Its body provides at the same time the target for WIMP-carbon nuclei collisions and the channel to direct those torn out nuclei towards the free end.

We present a first study of such a directional detector through the Monte Carlo simulation of WIMP collisions on the surface of CNTs and of the subsequent channeling of the recoiling carbon nuclei which exit the CNT at its open end.

We find that a detector assembled as an array of parallel CNTs would serve as a highly anisotropic and direction discriminating device. Different orientations of a CNT array with respect to the WIMP wind, give sensibly different channeling probabilities in the CNTs and therefore different ion counts at their free ends. Furthermore, CNTs are very efficient at channeling since they are rather empty channels: contrary to what happens in crystals, ions traveling through them

have very little interactions with electrons.

Our simulations are based on the calculation of the rate of nuclear recoils due to WIMP-nuclei interactions as a function of the nuclear final kinetic energy and recoil angle with respect to the WIMP wind direction. Integrating this distribution with respect to the recoil angle, we directly obtain the observable measured by DAMA/LIBRA. We confront our calculation with their experimental results. A remarkable agreement is reached by tuning the WIMP-nucleus coupling to the typical values discussed in the related literature. Tuning our model to DAMA/LIBRA data does not bind it logically to them. These are needed here only to discuss the outcome of our Monte Carlo simulations in some explicit, though hypothetical, context.

In a CNT at room or higher temperatures, carbon nuclei fluctuate around their equilibrium positions thus spending part of their time closer to the CNT axis. As we will explain in more detail, these are the conditions for a WIMP-nucleus scattering to be effective at channeling the carbon ions in the tube. We exploit our calculations of directional rates to finally compute how many counts per day (per Kg) are expected in terms of carbon ions emerging after channeling from an arbitrarily oriented CNT exposed to the WIMP wind.

This study shows that arrays of carbon nanotubes are a viable solution to the problem of directionality in direct dark matter searches.

Differently synthesised CNTs have different channeling properties and we show that a number of technological problems must be addressed in order to reach the optimal conditions to devise an efficient directional dark matter apparatus. Together with radiopurity issues, we will address these sort of problems in a forthcoming paper being confident of the way of controlling them.

In Section 2 we analyze the WIMP-nucleus scattering kinematics and obtain a compact formula for the directional rate of nuclear recoils. We also study the rate averaged over angles and, in Section 3, we confront it to the experimental results obtained by DAMA/LIBRA which are assumed as the hypothetical outcome of a non-directional experiment. Directionality is therefore studied at fixed values of the dark matter and nuclear masses. Section 4 is devoted to the discussion of the CNT as a channeling device and we introduce an algorithm to estimate its potentialities as an anisotropic detector. We show our results for different orientations of CNT with respect to the WIMP wind using the results obtained in Sections 2 and 3. In Section 5 we discuss an array of aligned CNTs and identify the most relevant technological problems to be solved to achieve an operative directional detector.

## 2 WIMP Wind Scattering Kinematics

Let  $\mathbf{v}$  be the velocity of the incident dark matter (DM) particle  $\chi$  and  $\mathbf{n}$  be the direction ( $|\mathbf{n}| = 1$ ) of the scattered nucleus  $\mathcal{N}$ . Define the frame in Fig. 1 with the  $z$ -axis along the Sun's direction.

In this frame the velocity vector

$$\mathbf{w}(t) \simeq [232 + 15 \cos \psi(t)] \mathbf{k} \quad (2.1)$$

is oriented along the Sun's direction and its length takes into account the velocity of the Earth around the Sun

$$\psi(t) = \left( 2\pi \frac{t - 152.5}{365.25} \right) \quad (2.2)$$

The  $\chi$  'wind' vector experienced by a detector at the origin of this frame will be  $-\mathbf{w}$ . The velocities are expressed in Km/sec and the time in days starting from January 1st. Here 232 Km/sec is the Sun's velocity along its Galactic motion. The value of 15 Km/sec is approximately equal to  $30 \text{ Km/sec} \times \cos 60^\circ$ , 30 Km/sec being approximately the velocity of the Earth along its motion around the Sun and  $60^\circ$  the inclination of the plane of the Earth's orbit with respect to the Sun's one.

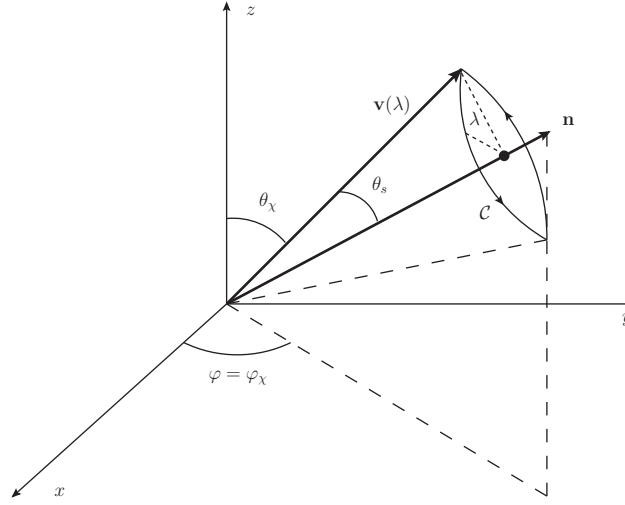


Figure 1: The  $z$  axis is in the direction of  $\mathbf{w}$  given in (2.1). The angle  $\theta_\chi$  is relative to the incoming dark matter (DM) particle  $\chi$ . The angles  $\theta(= \theta_\chi + \theta_s$  in figure) and  $\varphi$  define the direction of the recoiling nucleus  $\mathcal{N}$ , along  $\mathbf{n}$ , in the elastic scattering process  $\chi + \mathcal{N} \rightarrow \chi + \mathcal{N}$ . The  $\chi$  incident velocity  $\mathbf{v}$  in the figure has the same anomaly  $\varphi_\chi = \varphi$  of the scattered  $\mathcal{N}$ : we might fix it to  $\mathbf{v}_0 = \mathbf{v}(\lambda = 0)$  defining a direction to measure angles on the circle  $\mathcal{C}$ . The incoming DM particle direction is unknown but, as discussed in the text, if we fix the nucleus recoiling (kinetic) energy  $T$  and the incoming  $\chi$  velocity  $|\mathbf{v}|$ , the cone semi-aperture  $\theta_s$  gets fixed. Given  $T$  and  $|\mathbf{v}|$ , the  $\chi$  initial velocity vector tip will be somewhere on  $\mathcal{C}$ . Averaging out the initial  $\chi$  velocity direction translates into integrating the cross section, with some velocity distribution  $f(\mathbf{v})$ , along  $\mathcal{C}$  with variable  $\theta_s$ .

The velocity  $\mathbf{v}(\lambda)$  in Fig. 1 is given by

$$\mathbf{v}(\lambda) = \mathbf{v}_0 \cos \lambda + \mathbf{n}(\mathbf{n} \cdot \mathbf{v}_0)(1 - \cos \lambda) + (\mathbf{v}_0 \times \mathbf{n}) \sin \lambda \quad (2.3)$$

where we let  $\mathbf{v}_0 = \mathbf{v}(\lambda = 0)$  be that position of  $\mathbf{v}(\lambda)$  in which  $\varphi_\chi = \varphi$  and  $\theta = \theta_\chi + \theta_s$  with  $\theta_s < \pi/2$  (see Fig. 2). All other values are reached by varying  $\lambda \in [0, 2\pi]$ . The case depicted in figure is not

the only one possible, of course. Rotating  $\mathbf{n}$  at fixed  $\varphi$  in such a way that  $\mathbf{v}_0$  gets  $\varphi_\chi = \varphi + \pi$  and  $\theta = \theta_s - \theta_\chi$  produces the same expression for  $\mathbf{v}(\lambda)$ . Rotating  $\mathbf{n}$  in Fig. 1 in the same way (at fixed  $\varphi$ ) until  $\mathbf{v}_0$  is along  $\hat{z}$ , we have  $\varphi = \varphi_\chi$  when  $\lambda \rightarrow \lambda + \pi$ ; in this point  $\theta = \theta_\chi - \theta_s$ . This produces the same expression of  $\mathbf{v}(\lambda)$  as given before (it is essential that  $\theta_s < \pi/2$ ). At any rate, when  $\mathbf{v}_0$  is in the direction with  $\theta_\chi = 0$ , fixing  $\varphi_\chi = \varphi$  is not essential as  $\mathbf{v}_0$  has no  $\varphi_\chi$  dependency left. Similarly when  $\theta = 0$  there is no need to fix  $\varphi_\chi = \varphi$ .

We will eventually be interested in the line integral along  $\mathcal{C}$  of some velocity distribution  $f(|\mathbf{v}|)$  as given by

$$\int_{\mathcal{C}} f ds = \int_0^{2\pi} f(|\mathbf{v}(\lambda)|) \left| \frac{d}{d\lambda} \mathbf{v}(\lambda) \right| d\lambda = \sin \theta_s \int_0^{2\pi} f(|\mathbf{v}(\lambda)|) d\lambda \quad (2.4)$$

The factor  $\sin \theta_s$  found in the curvilinear integration, deriving  $\mathbf{v}(\lambda)$  with respect to  $\lambda$ , is indeed part of the  $d^3v$  velocity element which can be read by Fig. 1 to be

$$d^3v = (v \sin \theta_s d\lambda)(v d\theta_s) dv = (v^2 dv) d \cos \theta_s d\lambda \quad (2.5)$$

The  $\lambda$  integration is carried out at a *fixed*  $\theta_s$ , which means, as we will see below, that the nucleus recoiling kinetic energy  $T$  and incident velocity  $v$  are fixed.

With reference to Fig. 2 we can determine the expression for  $\cos \theta_s$  as a function of  $T$  (the recoiling nucleus energy),  $v$  and the mass  $\mu$  defined below. The scattering  $\chi + \mathcal{N} \rightarrow \chi + \mathcal{N}$  is elastic and non-relativistic. The momentum  $\mathbf{p}$  of the recoiling  $\mathcal{N}$  is given by (see Fig. 2)

$$2mv \sin \frac{\theta^*}{2} = |\mathbf{p}| \quad (2.6)$$

so that

$$2M_{\mathcal{N}}T = 4m^2v^2 \sin^2 \frac{\theta^*}{2} \quad (2.7)$$

or simply, since  $2\theta_s + \theta^* = \pi$ , where  $T$  is the recoiling nucleus *kinetic* energy

$$\frac{2T}{\mu v^2} = \sin^2 \frac{\theta^*}{2} = \sin^2 \left( \frac{\pi}{2} - \theta_s \right) = \cos^2 \theta_s \quad (2.8)$$

where

$$\mu \equiv \frac{4M_\chi^2 M_{\mathcal{N}}}{(M_\chi + M_{\mathcal{N}})^2} \quad (2.9)$$

Thus one obtains

$$\cos \theta_s = \sqrt{\frac{2T}{\mu v^2}} \quad (2.10)$$

whereas  $v_{\min} = \sqrt{2T/\mu}$ . Furthermore, fixing  $v$ , the  $d \cos \theta_s$  integration in  $d^3v$  corresponds to

$$d \cos \theta_s = \frac{1}{v \sqrt{2\mu T}} dT \quad (2.11)$$

so that

$$d^3v = v dv \frac{1}{\sqrt{2\mu T}} dT d\lambda \quad (2.12)$$

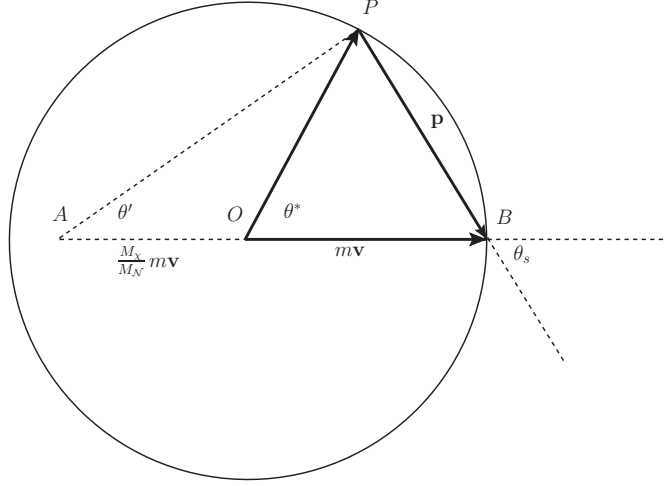


Figure 2: We are considering the non-relativistic elastic scattering of a DM particle  $\chi$  impinging on a nucleus  $\mathcal{N}$  initially at rest. The, non-relativistic, initial momentum of  $\chi$  in the centre of mass frame (COM) is therefore  $m\mathbf{v}$ , with  $m = (M_\chi M_\mathcal{N})/(M_\chi + M_\mathcal{N})$  being the reduced mass. After the elastic scattering has taken place, because of the conservation of kinetic energy, the initial incoming momentum  $OB$  is rotated by  $\theta^*$  (the COM scattering angle) into  $OP$ ,  $P$  being a generic point on the circle – the position of  $P$  fully characterises the scattering process. As is readily verified,  $AB = M_\chi \mathbf{v}$  coincides with the incoming momentum of  $\chi$  in the laboratory frame (LAB). Depending on  $M_\chi \gtrless M_\mathcal{N}$  the point  $A$  will lie outside/inside the disk of radius  $mv$ . On the other hand, the momentum of  $\chi$  after the scattering, in the LAB frame, is obtained by the velocity transformation  $\mathbf{k}' = m\mathbf{v}' + M_\chi \mathbf{V}$  where  $m\mathbf{v}'$  is the rotated vector  $OP$  and  $\mathbf{V}$  is the velocity of the COM,  $\mathbf{V} = M_\chi v/(M_\chi + M_\mathcal{N})$ . Thus  $\mathbf{k}' = m\mathbf{v}' + (M_\chi/M_\mathcal{N})m\mathbf{v} = AP$ . Moreover,  $PB = AP - AB = \mathbf{k}' - \mathbf{k} = \mathbf{p}$ ,  $\mathbf{p}$  being the momentum of the scattered nucleus in the LAB frame. The  $\theta_s (< \pi/2)$  angle is found between the initial LAB direction of  $\chi$  and the  $\mathcal{N}$  recoil momentum in the LAB.

where it is meant to integrate first in  $\lambda \in [0, 2\pi]$  with  $T, v$  constant, then in  $T$  with  $v$  constant and finally to integrate over  $v$ .

If  $n_\chi$  is the incident dark matter (DM) particle (number) density, we define an initial-velocity-averaged rate distributed in the solid angle  $d\Omega_{\mathbf{n}}$  relative to the recoiling nucleus direction as in Fig. 1

$$\frac{d\Gamma}{d\Omega_{\mathbf{n}}} := n_\chi \left\langle v \frac{d\sigma}{d\Omega_{\mathbf{n}}} \right\rangle_v \quad (2.13)$$

Using the standard formalism, the cross section distribution with respect to the solid angle  $d\Omega_{\mathbf{n}}$  where the nucleus recoils with energy  $E$  is, in the laboratory frame (and in the non-relativistic limit

for  $v \approx 10^{-3}c$ )

$$\begin{aligned}
\frac{d\sigma}{d\Omega_{\mathbf{n}}} &= \frac{1}{32\pi^2 M_{\mathcal{N}} |\mathbf{k}|} \int dE E \int \frac{d^3 k'}{2\mathcal{E}'} \delta^4(k - q - k') \sum_{\text{pol}} |\overline{M}|^2 = \\
&\equiv \frac{1}{32\pi^2 M_{\mathcal{N}} M_{\chi} v} \int dE E \int \frac{d^3 k'}{2\mathcal{E}'} \delta^4(k - q - k') \int d\mathcal{E}' 2\mathcal{E}' \theta(\mathcal{E}') \delta(k'^2 - M_{\chi}^2) \sum_{\text{pol}} |\overline{M}|^2 = \\
&= \frac{1}{32\pi^2 M_{\mathcal{N}} M_{\chi} v} \int dE E \delta(q^2 - 2\mathbf{k} \cdot \mathbf{q}) G_A^2 |F_A(\mathbf{q}^2)|^2 = \\
&\simeq \frac{1}{32\pi^2 M_{\chi} v} \frac{1}{(M_{\mathcal{N}} + M_{\chi})} G_A^2 |F_A(2M_{\mathcal{N}}T)|^2
\end{aligned} \tag{2.14}$$

where  $(\mathcal{E}, \mathbf{k})$  and  $(\mathcal{E}', \mathbf{k}')$  are related to the incident and scattered DM particle respectively.  $G_A$  is some unknown effective DM-nucleus interaction coupling whereas  $F_A(\mathbf{q}^2)$  is a nuclear form factor – both depend on the  $A$  nucleus involved. Here  $q$  is the transferred momentum  $q = k - k' = p' - p$ ,  $p$  and  $p'$  being the initial and final momenta of the nucleus  $p = (M_{\mathcal{N}}, \mathbf{0})$ ,  $p' = (E, \mathbf{p}')$ . Indeed  $\delta(q^2 - 2\mathbf{k} \cdot \mathbf{q}) = \delta(f(E))$  where

$$f(E) = 2M_{\mathcal{N}}(M_{\mathcal{N}} + \mathcal{E}) - 2E(M_{\mathcal{N}} + \mathcal{E}) + 2|\mathbf{k}||\mathbf{p}'| \cos \theta_s \tag{2.15}$$

and  $|\mathbf{p}'| = \sqrt{E^2 - M_{\mathcal{N}}^2}$ . The  $f(E) = 0$  equation has two roots. One is  $E_1 = M_{\mathcal{N}}$ , but  $1/|f'(E)|_{E_1} = 0$ . The other one is

$$E_2 = M_{\mathcal{N}} \frac{(\mathcal{E} + M_{\mathcal{N}})^2 + k^2 \cos^2 \theta_s}{(\mathcal{E} + M_{\mathcal{N}})^2 - k^2 \cos^2 \theta_s} \tag{2.16}$$

where  $k \simeq M_{\chi}v$ ,  $\mathcal{E} \simeq M_{\chi}$  (in the non-relativistic limit) and, using (2.9) and (2.10), we have  $E_2 = M_{\mathcal{N}}(2M_{\mathcal{N}} + T)/(2M_{\mathcal{N}} - T)$  and  $1/|f'(E)|_{E_2} = 1/(M_{\mathcal{N}} + M_{\chi})$ . Thus  $F(\mathbf{q}^2 = -2M_{\mathcal{N}}^2 + 2M_{\mathcal{N}}E)_{E=E_2} \simeq F(2M_{\mathcal{N}}T)$ <sup>1</sup>, since for low momentum transfers with respect to the mass  $M_{\mathcal{N}}$ ,  $q^2 \approx -\mathbf{q}^2$ .

Therefore we find

$$\frac{d\Gamma}{d\Omega_{\mathbf{n}}} = \frac{n_{\chi} G_A^2 F_A(2M_{\mathcal{N}}T)^2}{32\pi^2 M_{\chi} (M_{\mathcal{N}} + M_{\chi})} \int d^3 v f(\mathbf{v} + \mathbf{w}) \tag{2.17}$$

When adding  $\mathbf{w}$  to  $\mathbf{v}$  in the frame of Fig. 1 one gets  $\mathbf{v} + \mathbf{w}(t) = \mathbf{v}'$ , the latter being the velocity of DM particles in the Galactic frame, where they are supposed to obey a Maxwell-Boltzmann velocity distribution  $f(\mathbf{v}')$ .

The scattering amplitude does not depend on the scattering plane which is spanned by  $\mathbf{v}(\lambda)$  and  $\mathbf{n}$  in Fig. 1. Therefore we can choose  $\lambda = 0$ , place the vector  $\mathbf{k}'$  in that plane (with  $\theta'$  being the angle formed by  $\mathbf{k}'$  and  $\mathbf{k} = M_{\chi}\mathbf{v}_0$  – see  $\theta'$  in Fig. 2) and use the distribution  $d\sigma/d\Omega_{\mathbf{n}}$  computed. Therefore, returning to (2.17), we can write

$$\frac{d\Gamma}{dT d\cos \theta} = \frac{n_{\chi} G_A^2 F_A(2M_{\mathcal{N}}T)^2}{64\pi^2 M_{\chi}^2 \sqrt{2M_{\mathcal{N}}T}} \int_{\sqrt{2T/\mu}}^{v_{\max}} dv v \int_0^{2\pi} d\varphi \int_0^{2\pi} d\lambda f(\mathbf{v}(\lambda) + \mathbf{w}) \tag{2.18}$$

---

<sup>1</sup> $(-2M_{\mathcal{N}}^2 + 2M_{\mathcal{N}}E)_{E=E_2} = 4M_{\mathcal{N}}^2 T/(2M_{\mathcal{N}} - T)$ , where we can neglect  $T$  with respect to  $M_{\mathcal{N}}$  in the denominator.

where  $v_{\max} = 232 + 550 \text{ Km/sec}$  <sup>2</sup>.

The velocity distribution is defined by

$$f(\mathbf{v} + \mathbf{w}) = \beta e^{-\alpha(\mathbf{v} + \mathbf{w})^2} \quad (2.19)$$

where  $\alpha \sim 1/v_0^2, \beta \sim 1/v_0^3$  ( $v_0$  is usually taken to be  $v_0 \simeq 235 \text{ Km/sec}$ ), and the distribution peaks at  $\mathbf{v} = -\mathbf{w}$ , *i.e.* along the wind of  $\chi$  particles, see Eq. (2.1). Therefore we have

$$f(\mathbf{v} + \mathbf{w}) = \beta e^{-\alpha(A(t) + B(t) \cos \lambda)} \quad (2.20)$$

where, using Eq. (2.3), we obtain

$$A(t) = v^2 + w^2(t) + 2v \cos \theta_s \cos \theta w_z(t) \quad (2.21)$$

$$B(t) = 2v \sin \theta_s \sin \theta w_z(t) \quad (2.22)$$

using the formula for  $\mathbf{w}$  in (2.1). Observe that there is no dependency left on the  $\varphi$  angle.

Incidentally, we note that a reduction in terms of the modified Bessel function of the first kind is possible

$$\int_0^{2\pi} d\lambda e^{-\alpha(A(t) + B(t) \cos \lambda)} = 2\pi e^{-\alpha A(t)} I_0(\alpha B(t)) \quad (2.23)$$

so that <sup>3</sup>

$$\frac{d\Gamma}{dT d\cos\theta} = \frac{n_\chi G_A^2 F_A (2M_N T)^2}{16M_\chi^2 \sqrt{2M_N T}} \int_{\sqrt{2T/\mu}}^{v_{\max}} dv v \beta e^{-\alpha A(t)} I_0(\alpha B(t)) \quad (2.24)$$

The non-relativistic kinematics of the DM-nucleus scattering involves the factorization of the nuclear form factor so that the angular distribution is universal, depending only on the Maxwell-Boltzmann assumption of the DM velocity distribution.

The  $d\Gamma/dT$  distribution, which can be obtained from (2.24) by integration over  $\cos\theta$ , is a function of time through  $w_z(t)$  defined in (2.1). This can be numerically expanded in a Fourier trigonometric series whose cos and sin harmonics of  $\psi(t)$  can be studied. One observes that the model

$$\frac{d\Gamma}{dT} = Q(T) + S(T) \cos \psi(t) \quad (2.25)$$

---

<sup>2</sup>The escape velocity at the Solar System's galactic radius with respect to the Milky Way's gravity is  $\approx 550 \text{ Km/sec}$ . The Maxwell-Boltzmann velocity distribution in the Galactic frame is sharply limited at  $v_{\max}$  by a factor  $\theta(v_{\max} - V)$ . In the calculation of the rate (2.24) we have  $V = v + w$  so that  $v_{\max} - w = v_{\text{esc}} = 550 \text{ Km/sec}$  thus allowing  $v_{\max} \approx 780 \text{ Km/sec}$ .

<sup>3</sup>We use  $M_\chi, M_N = \# \text{ GeV}$ ,  $T = \# \text{ KeV}$ ,  $n_\chi = \# \text{ cm}^{-3}$ . We wish to express the velocities in  $\text{Km/sec}$ : this means that we make the substitution  $u = c \cdot v$  and accordingly rescale the  $\beta$  factor by  $c^3$ . Then the result of the integral will be  $\# (\text{sec/Km}) \cdot c$ . In order to express  $d\Gamma/dT d\cos\theta$  in units of  $1/\text{KeV} \cdot \text{sec}$  we have to include an overall constant of  $K_1 = 3.5 \times 10^{-15}$  on the rhs of (2.24). The local dark matter density is estimated to be  $\rho_\chi = 0.3 \pm 0.1 \text{ GeV} \cdot \text{cm}^{-3}$ . For a  $M_\chi = 100 \text{ GeV}$  dark matter particle we would have  $n_\chi = 0.003 \text{ cm}^{-3}$ . Newer results show  $\rho_\chi = 0.9 \pm 0.5 \text{ GeV} \cdot \text{cm}^{-3}$ . To make comparisons with the results shown by the DAMA experiment,  $d\Gamma/dT$  has to be multiplied by the number of target nuclei per kilogram  $N_T = N_A/MW$ , where  $MW$  = molecular weight of the detector. In that case  $MW = 149.9 \text{ gr/mole}$  and  $N_T = 4 \times 10^{24} \text{ kg}^{-1}$ . Therefore, to express  $d\Gamma/dT$  in counts per day we have to include a constant factor of  $K_2 = 35 \times 10^{28} \text{ Kg}^{-1}$ . The overall constant to include is therefore  $K_1 K_2 = 1.22 \times 10^{15} \text{ Kg}^{-1}$ . The mass of the DAMA detector is  $250 \text{ Kg}$ .



is a very good approximate description, exception made for a small range of kinetic energies  $T$  (few KeVs when comparing to DAMA data; see Fig. 4). At the boundaries of this interval the function  $S(T)$  has to be taken with opposite signs whereas other harmonics are required to reconstruct  $d\Gamma/dT$  in between – the net amplitude of the oscillation gets smaller when approaching some  $T^*$  from lower or higher values of  $T$ . The behavior of the  $S(T)$  function will be further discussed in the next Section.

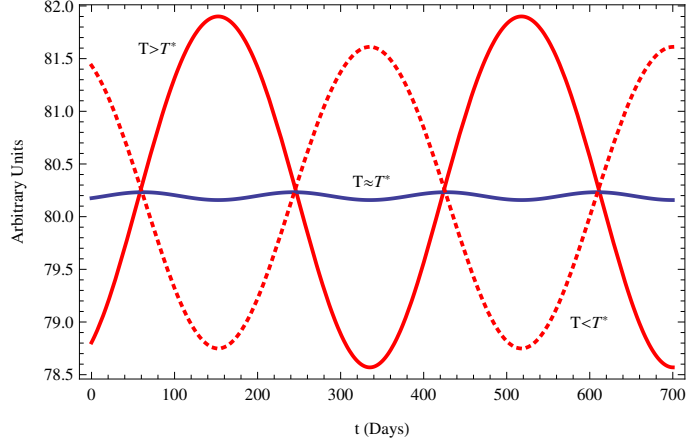


Figure 3: Choosing the same offset for three  $d\Gamma/dT$  distributions computed for  $T > T^*$  (solid, red),  $T \approx T^*$  (solid, blue),  $T < T^*$  (dotted, red), we see that passing through the  $T^*$  point,  $d\Gamma/dT$  gets smaller in amplitude and  $S(T)$  in (2.25) has to be reversed in sign. When  $T \geq T^*$  the oscillation has essentially the same frequency  $\omega$  as in  $\psi(t)$  given in (2.2). The frequency  $\omega$  can effectively become twice as large for  $T \approx T^*$ .

As for the form factor, following the standard assumptions made in the literature [5], we use the Helm function

$$F(q) = 3 e^{-q^2 s^2/2} \frac{\sin(qr_n) - qr_n \cos(qr_n)}{(qr_n)^3} \quad (2.26)$$

where  $s \simeq 0.9$  fm and  $r_n = c^2 + (7/3)\pi^2 a^2 - 5s^2$  is an effective nuclear radius with  $a \simeq 0.52$  fm and  $c \simeq 1.23A^{1/3} - 0.60$  in units of fermis;  $q$  is given by  $q = \sqrt{2m_N T}$ .

### 3 Annual Modulation and Directionality

As thoroughly discussed in the literature, see *e.g.* [5], the  $\chi\mathcal{N}$  spin-independent cross section can be written as

$$\sigma_{\chi\mathcal{N}} = \frac{\mu_{\chi\mathcal{N}}^2}{\mu_{\chi p}^2} A^2 \sigma_{\chi p} \quad (3.1)$$

where, in the case we are considering  $M_\chi \approx M_N$

$$\mu_{\chi\mathcal{N}} = \frac{M_\chi M_N}{(M_\chi + M_N)} \quad (3.2)$$

$$\mu_{\chi p} = \frac{M_\chi M_p}{(M_\chi + M_p)} \approx M_p \quad (3.3)$$

so that (3.1) can be written as

$$\sigma_{\chi\mathcal{N}} = \frac{\mu_{\chi\mathcal{N}}^2}{M_p^2} A^2 G^2 \Lambda^2 \quad (3.4)$$

where  $G$  is some coupling with dimensions of  $\text{GeV}^{-2}$  and  $\Lambda$  is some energy scale which we might fix to  $\Lambda \approx M_\chi$ .  $A$  is the nucleus  $\mathcal{N}$  mass number. From (2.14) we see that we are using a

$$\sigma_{\chi\mathcal{N}} \sim \frac{1}{M_\chi(M_\chi + M_N)} A^2 G^2 \Lambda^4 \quad (3.5)$$

Comparing (3.4) with (3.5)

$$G_A = A G \frac{\mu_{\chi\mathcal{N}}}{M_p} \Lambda^2 \quad (3.6)$$

with  $\Lambda \approx m_\chi$ . We can then use (3.6) in the expression for the rate (2.24). To compare  $S(T)$  defined in Eq. (2.25) to data shown by the DAMA collaboration, we estimate

$$\sigma_{\chi p} \approx G^2 M_\chi^2 \approx 10^{-5} \text{ pb} \quad (3.7)$$

in agreement with what reported in [5].

In Fig. 4 we compare our calculation of  $S(T)$  as from Eqs. (2.25,2.24) with experimental results provided by the DAMA collaboration. We underscore that, apart from a small region of  $T$  values around the point where  $S(T)$  crosses the  $y = 0$  axis, the model (2.25) is generally valid.

With the same parameter values we can compute the angular distributions (2.24), reported in Fig. 5, for a set of different recoil kinetic energies from  $T = 1$  to  $T = 100$  KeV. The different curves are equally normalized to their maxima in order to show them on the same plot. An asymmetry parameter  $A$  can be defined starting from the plot in Fig. 5

$$A = \frac{I(\cos \theta > 0) - I(\cos \theta < 0)}{I(\cos \theta > 0) + I(\cos \theta < 0)} \quad (3.8)$$

where  $I$  are the integrals of the distributions found. The asymmetry  $A$  varies with recoil kinetic energy as reported in Fig. 6 (left panel). Finally, in Fig. 6 (right panel) we report the total rate computed in (2.25) as compared to the one measured by DAMA.

This completes the tuning of our computation to DAMA results, used as a benchmark to devise the simulations presented in the next Section. Having fixed the parameters we will use what found on the  $d\Gamma/dT d\cos \theta$  distribution to generate a sample of Monte Carlo WIMP-nucleus scattering events to test the potentialities of carbon Nanotubes as channeling devices for directional dark matter searches. Namely we use  $d\Gamma/dT d\cos \theta$  as a probability distribution to randomly generate

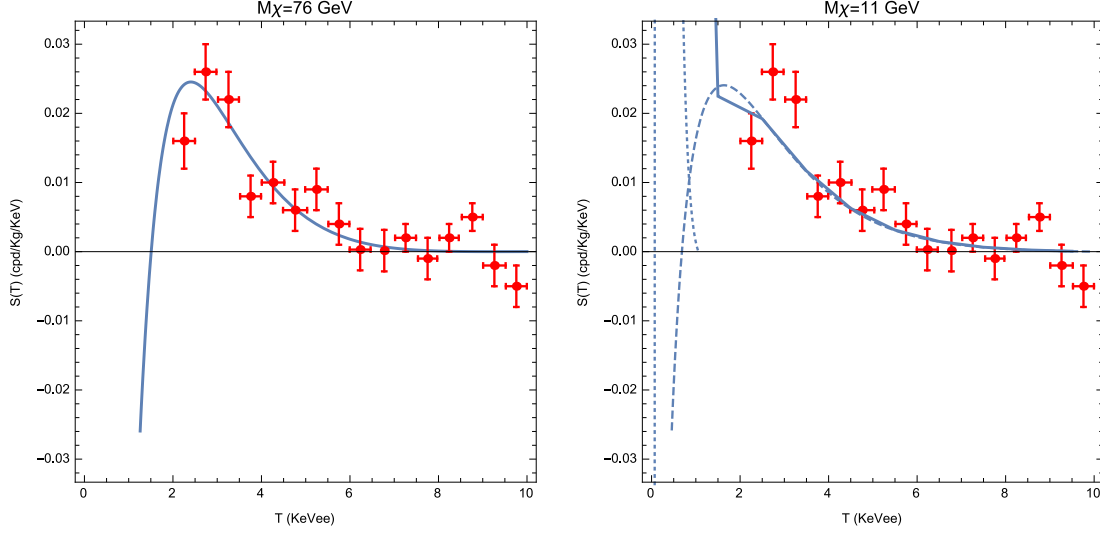


Figure 4: Comparison of the  $S(T)$  function in (2.25) with the experimental results provided by the DAMA collaboration. Quenching factors  $Q$  for sodium and iodine are used to rescale the  $T$  axis in the units of KeVee,  $T(\text{KeVee}) = T(\text{KeV})/Q$ . Namely  $Q_I = 11$  and  $Q_{Na} = 3.3$ . On the left panel we use a WIMP mass of  $M_\chi = 76$  GeV. In that case iodine recoil dominates and  $\sigma_{\chi p} \simeq 3.2 \times 10^{-5}$  pb. On the right panel  $M_\chi = 11$  GeV ( $\sigma_{\chi p} \simeq 3 \times 10^{-4}$  pb) and both contributions from sodium and iodine have to be considered. Iodine (dotted curve) takes over at low values of nucleus recoil energy (reaching a maximum at  $\approx 1$  cpd). Sodium contribution to the modulation amplitude is shown by the dashed curve. The solid curve is a combined histogram of the two contributions with a bin size (experimental resolution) of 1 KeV in the range  $[0, 5]$  keV. In the region of kinetic energies where  $S(T)$  changes sign, the model (2.25), as commented in the previous Section, is not strictly applicable.

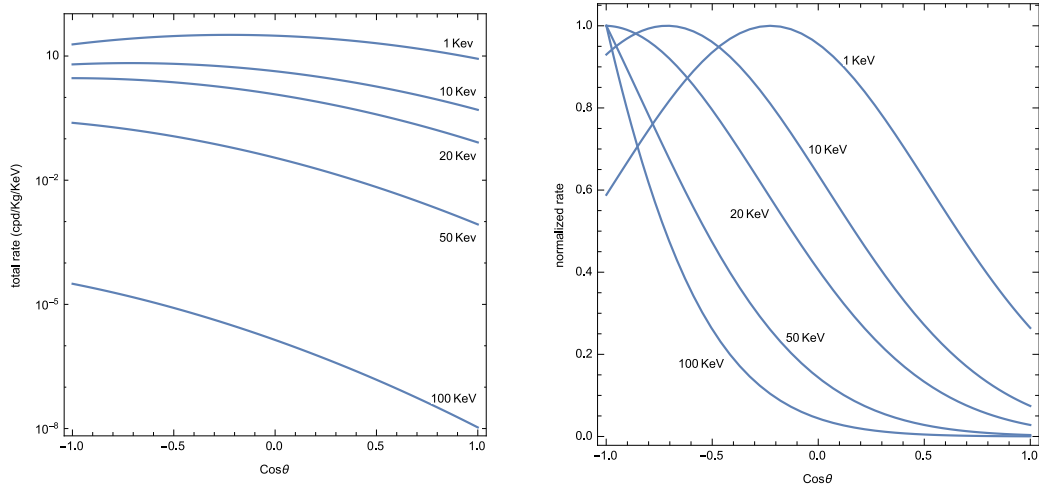


Figure 5: Left Panel: Angular distributions in the  $\cos \theta$  variable,  $\theta$  being the angle of the recoiling nucleus with respect to the Sun direction at the scattering time. Different values of  $T$  correspond to different values of recoiling nuclei kinetic energies. Right Panel: Same as left panel using the same normalization for different recoil kinetic energies. The variation with time is found to be negligible

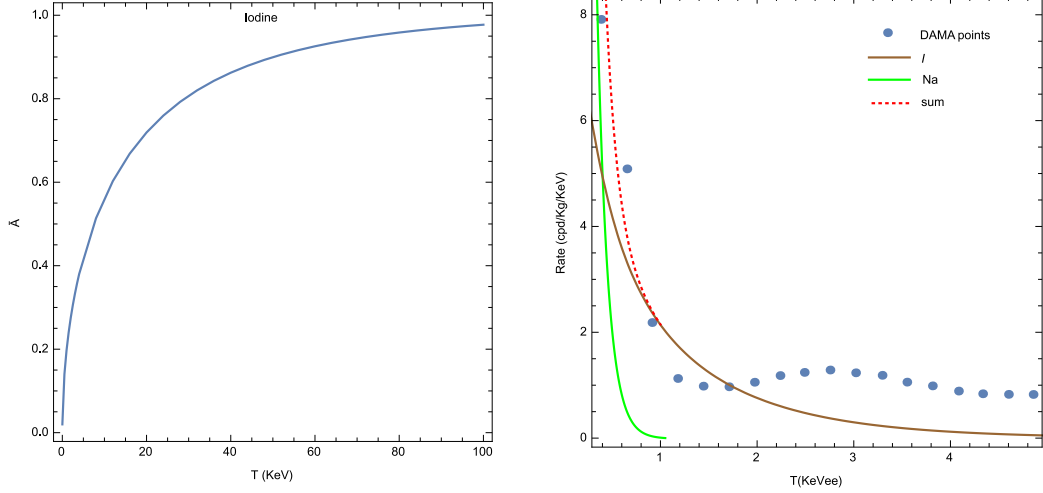


Figure 6: Left Panel: The Asymmetry parameter  $A$  for the iodine, introduced in Eq. (3.8). Right Panel: The total rate (2.25) obtained as compared to the DAMA total rate.

events of recoiled nuclei carrying kinetic energy  $T$  with a scattering angle with respect to the WIMP wind direction of  $\theta$ . Thus we generate a sample of  $(T, \theta)$  pairs. In particular we will focus on the low mass window  $M_\chi \approx 10$  GeV, but our results are easily reproduced for other WIMP mass values. Carbon nuclei,  $A = 12$ , should be recoiled quite effectively by such WIMPs.

## 4 Conceptual Study of a carbon Nanotube Directional Detector

We propose a new type of directional detector for direct Dark Matter searches based on a large array of carbon Nanotubes (CNT). We shall present here an initial study of the efficiency of this apparatus at discriminating the WIMP wind direction.

As shown in Fig. 7, a WIMP collides with the surface of a carbon Nanotube in point  $A$ , extracting a carbon nucleus from it. This might be kicked inside the nanotube and, provided it has the correct parameters in terms of kinetic energy  $T$  and direction  $\theta$  (with respect to the CNT axis), it will be *channeled* in the CNT, a phenomenon similar to total reflection in an optic fiber. The carbon nucleus eventually reaches one of the two ends of the CNT. Actually, because of *crystal blocking*, to be discussed below, the carbon nucleus has a chance of being channeled only if it is struck by the WIMP while its position fluctuates inward due to thermal vibrations.

On the basis of the recoil distributions  $d\Gamma/dT d\cos\theta$ , we would roughly expect that a CNT oriented along the WIMP wind direction ( $\hat{z}$  axis in Fig. 1) will channel more effectively the hit carbon nuclei with respect to the case in which the nanotube is oriented perpendicularly to the WIMP wind, see Fig. 5<sup>4</sup>. Once the channeled carbon ion has escaped the CNT, it is collected and registered by a drift detector (point  $B$  in Fig. 7).

<sup>4</sup>actually the analog of Fig. 5 for carbon nuclei.

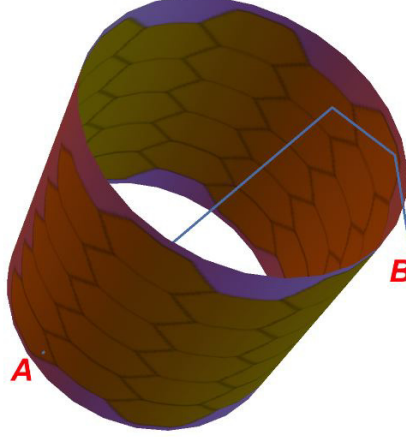


Figure 7: The WIMP particle hits a carbon nucleus of the nanotube in  $A$ . The carbon nucleus can recoil within the nanotube and have the correct parameters to be totally reflected within the CNT until it escapes in  $B$ .

The carbon nucleus injected in the CNT experiences an effective axial potential (energy) along its transverse motion (with respect to the CNT axis) given by [6]

$$U(r, \phi) = U_0(r) + 2 \sum_{s=1}^{\infty} U_{sN}(r) \cos \frac{\pi s(n+m)}{q} \cos \left( sN\phi + \frac{\pi s(n+m)}{q} \right) \quad (4.1)$$

where cylindrical coordinates  $(r, \phi)$  are used. The  $U_{\nu}(r)$  terms,  $\nu = 0, 1, 2, \dots$ , are independent of the  $\phi$  angle taken from the center of the potential – they have a cylindrical symmetry. It is found that

$$U_{\nu}(r) = 4\sqrt{\pi}\sigma Z^2 e^2 \left( \frac{R}{r} \right)^{1/2} \sum_{j=1}^4 a_j b_j e^{-b_j^2(r^2+R^2)} e^{2b_j^2 r R [\sqrt{1+\xi^2} - \xi \ln(\xi + \sqrt{1+\xi^2})]} \quad (4.2)$$

where  $\xi = \nu/(2b_j^2 r R)$  and Gaussian units are used ( $\alpha = e^2/\hbar c$ );  $r$  assumes values from 0, the center of the potential, to the surface of the CNT at  $r = R$ . Here  $\sigma = 4/(\ell^2 \sqrt{27})$  where  $\ell \simeq 0.14$  nm is the bond length between carbon atoms and

$$\begin{aligned} a_j &= (3.222, 5.270, 2.012, 0.59499) \times 10^{-4} \text{ nm}^2 \\ b_j &= (10.33, 18.694, 37.456, 106.88) \text{ nm}^{-1} \end{aligned} \quad (4.3)$$

as reported in [6]. The exponential function in the sum in (4.2) reduces to  $e^{-b_j^2(R-r)^2}$  when  $\nu = 0$ .

The CNT are characterized by a *roll-up* vector  $\mathbf{r}_0 = n\mathbf{a} + m\mathbf{b}$ , where  $n, m$  are two integers, the CNT indices, and  $\mathbf{a}, \mathbf{b}$  are the basis vectors of a graphite plane (the angle between  $\mathbf{a}$  and  $\mathbf{b}$  is  $\pi/3$  and  $|\mathbf{a}| = |\mathbf{b}| = \ell\sqrt{3}$ ). The nanotube is a rolled up strip of width  $|\mathbf{r}_0|$  cut out by a graphite carbon plane perpendicularly to  $\mathbf{r}_0$ . The resulting cylinder is closed (at either end) with caps containing carbon pentagons in a manner that conserves bonding length. The radius  $R$  of a CNT is

$$R = \frac{\ell\sqrt{3}}{2\pi} \sqrt{n^2 + nm + m^2} \quad (4.4)$$

A nanotube  $(n, m)$  can be represented as a collection of  $2N$  rows parallel to the tube axis and it is found that

$$N = \frac{2}{q}(n^2 + nm + m^2) \quad (4.5)$$

where  $q = \gcd(2m + n, 2n + m)$ . These equations fully define Eq. (4.1).

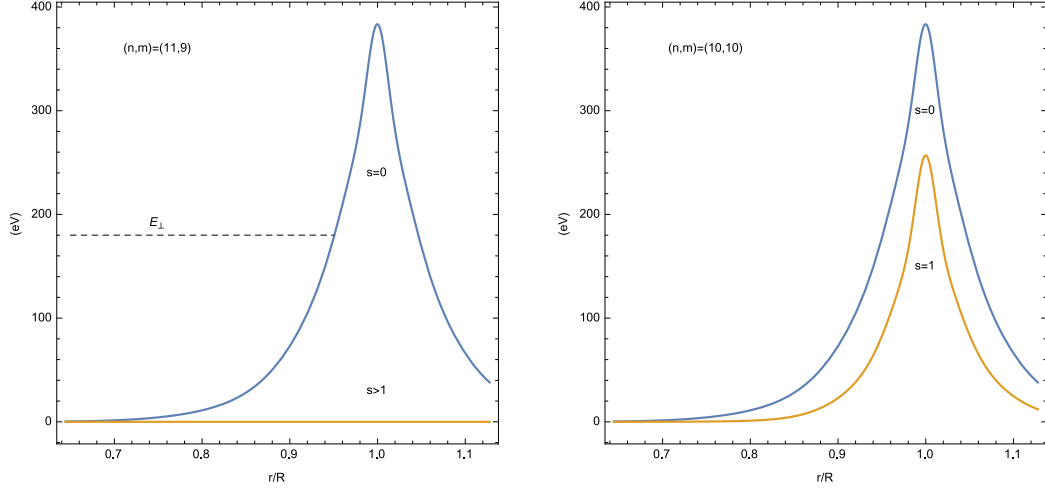


Figure 8: Left Panel: (11, 9) CNT. The profile of  $U_0$ , ( $s = 0$ ), versus that of  $U_{602}$ , ( $s = 1$ ). The effective potential  $U(r, \phi) = U(r)$ . Right Panel: The profile of  $U_0$ , ( $s = 0$ ), versus that of  $U_{20}$ , ( $s = 1$ ). The effective potential in (4.1) depends also on  $\phi$  as is always the case for  $n = m$  or  $n \vee m = 0$  CNT.

The essence of the channeling phenomenon is the existence of a classical turning point as in Fig. 8, left panel. In other words the total transverse energy  $E_\perp$  of the ion kicked inside the CNT by the WIMP, should not exceed the effective potential barrier at  $r \approx R$  for the ion to be channeled. In the Lindhard theory of channeling another condition is required [7]: if  $x$  is the distance from the nanotube surface,

$$U''(x) < \frac{8T}{(\ell \cos(\pi/3))^2} \quad (4.6)$$

which we find is verified for every  $x$  in the range of kinetic energies  $T$  we consider.

In Fig. 8 we show how for certain CNT, for example the (11, 9) on the left panel, the higher  $U_{\nu>0}$  terms are irrelevant and the effective potential has cylindrical symmetry. In other cases, consider for example the CNT (10, 10) on the right panel (or in general  $n = m$  or  $m \vee n = 0$  nanotubes), the higher terms are important and  $U(r \approx R, \phi)$  of Eq. (4.1) has an explicit dependence on  $\phi$ , showing a periodical sequence of maxima and minima, see Fig. 9.

Therefore, besides some particular cases, the motion of the ion in the transverse direction is subject to a potential  $U(r, \phi)$  with a sinusoidal  $\phi$  dependency. This means that the  $v_\phi = r\dot{\phi}$  component of the carbon ion transverse velocity will change when approaching  $r \approx R$ , and the transverse angular momentum will not be an integral of motion. On the other hand, for CNT like the (11, 9) of Fig. 8, a centrifugal barrier prevents channeled trajectories (those having  $E_\perp$  lower

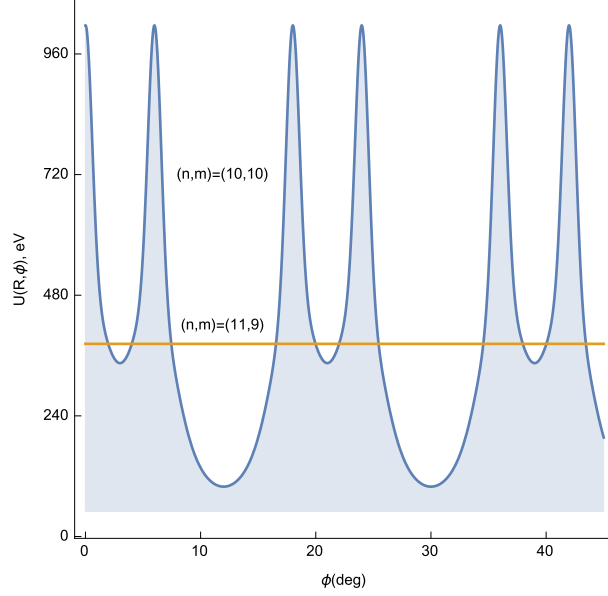


Figure 9: The  $\phi$  dependence of the effective potential  $U(R, \phi)$  at the nanotube surface  $r \simeq R$  in the case of the (10,10) CNT as compared to the (11,9) one. The (10,10) nanotube clearly shows some ‘holes’ with respect to the (11,9) one (see the region around  $\phi \sim 10^\circ$  or  $\phi \sim 30^\circ$ ) with the consequence of being less effective at channeling.

than the barrier at  $R$ ) to get close to the CNT axis and the classical motion is expected to be confined in a circular crown between some  $r_{\min}$  and  $R$ .

The temperature of the system,  $T^*$ , might also be taken into account when deriving the effective potential  $U(r, \phi)$ . However, it is shown that the influence of thermal vibrations is relatively small in the definition of function  $U(r, \phi)$ .

On the other hand, at finite  $T^*$ , each single carbon site undergoes transverse thermal fluctuations (longitudinal ones are irrelevant here), bringing it toward the inside (or the outside) of the CNT. The one-dimensional amplitude of thermal fluctuations in Debye theory is given by  $u_1(T^*) \approx 10^{-2}$  nm at room temperature. As discussed in the context of crystals [8], due to lattice vibrations the collision with a WIMP may happen while a carbon site, in our case, is far enough within the interior of the channel. This is essential to channeling: if channeled ions never go close to lattice sites the reversed paths do not happen either.

To check the channeling conditions starting from a  $(T, \theta)$  nucleus recoil event, we compute the transverse kinetic energy  $T(\sin \theta)^2$  and require that the total transverse energy

$$E_{\perp} = T(\sin \theta)^2 + U(R - x, \phi) \lesssim \min U(R, \phi) \quad (4.7)$$

This provides a  $x_{\min}$  minimum value for  $x$ . The probability (weight of the event) that the carbon

nucleon which recoiled with  $\approx T\theta^2$  is channeled is given by

$$\mathfrak{w}(T, \theta) = \int_{\mathcal{R}} dx dy \frac{e^{-x^2/2u_{\perp}^2(T^*)}}{\sqrt{2\pi}u_{\perp}(T^*)} \frac{e^{-y^2/2u_{\parallel}^2(T^*)}}{\sqrt{2\pi}u_{\parallel}(T^*)} \quad (4.8)$$

where, see Fig. 10

$$\mathcal{R} := l^2 - 2lR \cos \psi < x_{\min}^2 - 2x_{\min}R \quad (4.9)$$

and

$$l = \sqrt{x^2 + y^2} \quad \text{and} \quad dx dy = l dl d\psi \quad (4.10)$$

whereas the average radial and longitudinal vibration amplitudes (as described in Debye theory) are given by

$$\begin{aligned} u_{\perp} &= 0.0085 \text{ nm} \\ u_{\parallel} &= 0.0035 \text{ nm} \end{aligned} \quad (4.11)$$

We therefore obtain the number of counts per day per Kilogram of channeled carbon nuclei expected

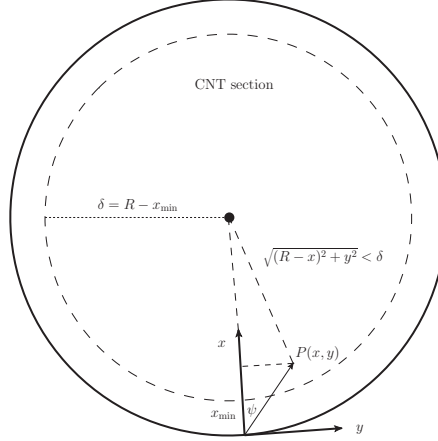


Figure 10: Due to lattice vibrations, a carbon site fluctuates from the CNT surface to point  $P$ . For channeling to take place, point  $P$  has to be in a disk of radius  $R - x_{\min}$ . The WIMP-carbon scattering is supposed to occur in point  $P$ .

in a CNT using *i*) the distribution (2.24) tuned on DAMA data and *ii*) the Monte Carlo calculation outlined in (4.7) and (4.8). Namely we produce samples of  $(T, \theta)$  events generated randomly as prescribed by the tuned distribution (2.24). To each of them we attach the probabilistic weight  $\mathfrak{w}(T, \theta)$  and finally compute the histogram of channeled events as in Fig. 11 – left panel – using three orientations for the CNT:  $\theta = \pi$ , base to open cap of the CNT in the WIMP wind direction ( $-\mathbf{w}$  of Eq. (2.1)),  $\theta = \pi/2$ , orthogonal to it and  $\theta = 0$ , base to open cap opposite to the WIMP wind. In the right panel of Fig. 11 we also show the  $\cos \theta$  dependency as a function of the operating temperature of the CNT. In both left and right panels of Fig. 11 the CNT is supposed to be oriented *along* the  $z$ -axis of Fig. 1.



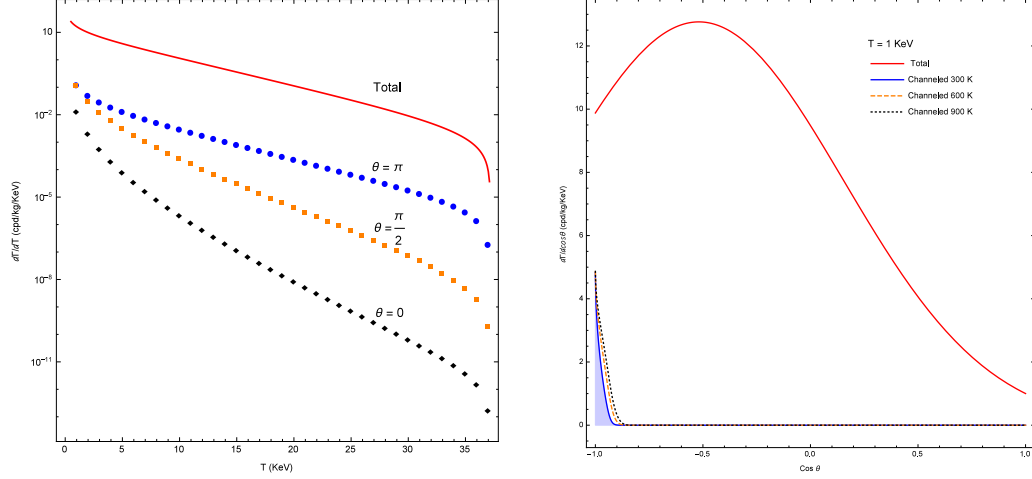


Figure 11: Left Panel: Expected histogram of counts of channeled carbon nuclei in a CNT oriented along the WIMP wind direction, with the direction from the base to the open cap along  $-\hat{z}$ , indicated as  $\theta = \pi$ , orthogonally to it  $\theta = \pi/2$  and with  $\theta = 0$ , as a function of the nucleus recoil kinetic energy  $T$ . Right Panel:  $d\Gamma/d\cos\theta$  distribution as a function of the temperature of the CNT for a specific value of the recoil nucleus kinetic energy.

## 5 CNT Aligned Arrays

As illustrated in the previous Section, a CNT exhibits an *anisotropic response* to the interaction of a heavy dark matter particle with carbon nuclei. When parallel to the average WIMP wind direction, a fraction of carbon nuclei scattered off their own nuclear sites are channeled, while those

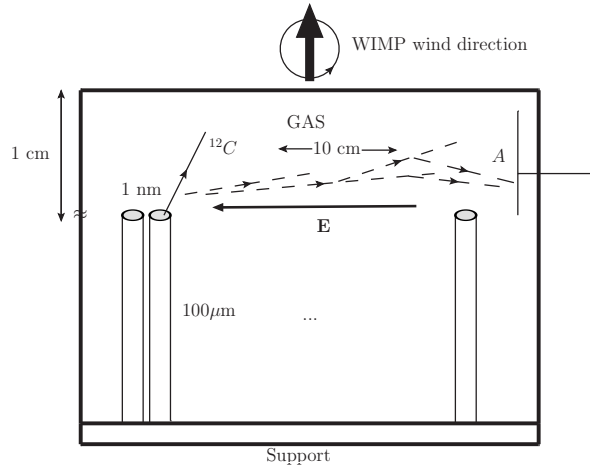


Figure 12: Sketch of the CNT array detector. The Gas pressure in the cell might be tuned at low values in such a way to prevent the gas to be adsorbed on to the nanotubes surfaces. Heating the substrate helps at keeping clear the nanotube channels. The optimization of these parameters will be considered in a forthcoming publication.

emitted in other directions are preferably absorbed by the CNT.

A channeled carbon ion can be stopped in a few cm thick gas volume at the CNT end point. It will release (at least part of) its kinetic energy by ionizing the gas. The electrons produced can be guided to an Anode by an electric field. A proportional amplification takes place which allows the measurement of the carbon ions initial kinetic energy.

This scheme of detection is described in Fig. 12, where an array of aligned CNTs is used as the massive target for WIMP scattering. The length of the CNT array should be of the order of  $100\text{ }\mu\text{m}$ . However, this must be further optimized to reduce the effect of ion dechanneling, on one hand, and to absorb the ions scattered away from the CNT axis, in order to preserve the information of the dark matter direction, on the other.

Arrays of CNTs can easily be synthesized with a good alignment quality on various substrates [9]. In our conceptual design the substrate should be thick enough to absorb any scattered particles out of the CNT, when the direction is opposite to the WIMP wind. Notice that CNTs, closely packed and aligned, might allow a larger channeling efficiency since ions leaving one tube may be rechanneled in another tube. This might be obtained from CNT ropes suitably cut and oriented [10].

Approximately  $10^{16}$ ,  $\varnothing = 1\text{ nm}$  diameter CNTs, can fit on a  $10\times 10\text{ cm}^2$  substrate. Since the surface density of a graphene sheet is [11]  $1/1315\text{ g/m}^2$ , about 2 grams of CNT can be packed on the substrate.

This detector element, composed by the CNT array target and the electron drift gas region, might easily be reproduced on large layers in a modular way. Several layers could then be piled-up to reach a  $\approx 10\div 100\text{ Kg}$  mass in a relatively limited space.

Radiopurity of the components of such dark matter detectors should carefully be evaluated. One intrinsic source of background is the presence of  $^{14}\text{C}$  within the CNT walls.  $^{14}\text{C}$  exhibits a  $\beta$  decay with a spectrum endpoint at  $156\text{ KeV}$  and a half-time of about 5740 years. The abundance of  $^{14}\text{C}$  in terrestrial carbon is  $\sim 10^{-11}$  and has a cosmogenic origin from the nuclear transmutation of  $^{14}\text{N}$  into  $^{14}\text{C}$  due to cosmic rays. On the other hand, there are indications [12] that organic compounds have isotopic abundances of  $^{14}\text{C}$  as low as  $10^{-18}$  having originated from petroleum which has not been exposed to cosmic rays for millions of years. If CNTs are made from organic gases originating from such pure precursors, the level of such background might be well under control. Furthermore,  $100\text{ }\mu\text{m}$  long CNTs would help in absorbing most  $\beta$  electrons. In this respects, an effect that must be evaluated is the fraction of  $\beta$  particles being channeled by a CNT.

A detailed study of the ion detection system and of backgrounds is the subject of another paper in preparation.

## 6 Conclusions

We presented a new detector for directional dark matter searches and analyzed its potentialities through a Monte Carlo study of its fundamental unit: a single wall carbon nanotube having a variable orientation with respect to the WIMP wind.

A WIMP with a mass of approximately 10 GeV and a velocity  $\approx 220$  Km/sec would be very effective at kicking a carbon nucleus out of its lattice site on the nanotube surface. If directed toward the interior of the tube, there is a probability that the carbon ion is channeled, a sort of total reflection phenomenon that drives the ion along the carbon nanotube direction. Of course, heavier (or lighter) WIMPs might also be detected and produce channeled events, as can straightforwardly be estimated with the method presented here.

The ion might reach the open end of the tube and exit from it – all this depends on the orientation of the nanotube with respect to the WIMP wind in a way that we have computed explicitly, see Fig. 11 (left panel). The input of our calculation is the directional recoil rate tuned on DAMA/LIBRA data, see Figs. 4 and 6, in order to control our simulation on a physical, although controversial case.

The carbon nanotube array detector might detect WIMPs also giving information on their original direction. The kinetic energy of the recoiling nucleus, to be reconstructed by the apparatus, can be correlated to the channeling probability and the mass of the WIMP itself can be estimated by a comparison with the expected counts.

In a forthcoming publication we plan to provide a study on the full treatment of the background and of the reconstruction of the signal in the apparatus schematically represented in Fig. 12.

## Acknowledgements

We wish to thank M Diemoz for having stimulated our interest on this topics and P Lipari for a thorough introduction on the subject of directionality and for his collaboration in the early stages of this work. We also thank C Savage for a useful response in answer to our queries. We thank C Mariani, MG Betti and A Polimeni for interesting discussions on carbon nanotubes and nanowires and S Orlanducci and ML Terranova for providing information on the synthesis of CNTs.

## References

- [1] R. Bernabei *et al.* [DAMA Collaboration], Eur. Phys. J. C **56**, 333 (2008) [arXiv:0804.2741 [astro-ph]].

- [2] D. S. Akerib *et al.* [LUX Collaboration], Phys. Rev. Lett. **112** (2014) 9, 091303 [arXiv:1310.8214 [astro-ph.CO]].
- [3] R. Bernabei, P. Belli, F. Montecchia, F. Nozzoli, F. Cappella, A. Incicchitti, D. Prosperi and R. Cerulli *et al.*, Phys. Rev. D **77**, 023506 (2008) [arXiv:0712.0562 [astro-ph]].
- [4] See talk by Dinesh Loomba in the 42nd SLAC Summer Institute, *Shining Light on Dark Matter*, <https://indico.cern.ch/event/297618/other-view?view=standard> and S. Burgos *et al.*, Astropart. Phys. **31** 261-266 (2009).
- [5] K. Freese, M. Lisanti and C. Savage, Rev. Mod. Phys. **85**, 1561 (2013) [arXiv:1209.3339 [astro-ph.CO]].
- [6] N.K. Zhevago and V.I. Glebov, Journal of Experimental and Theoretical Physics, Vol. 91, No. 3 (2000), pp. 504-514; see also X. Artru, S. P. Fomin, N. F. Shulga, K. A. Ispirian and N. K. Zhevago, Phys. Rept. **412**, 89 (2005).
- [7] J. Lindhard, Kongel. Dan. Vidensk. Selsk. Mat.-Fys. Medd. **34**, No. 14 (1965).
- [8] G. B. Gelmini, J. Phys. Conf. Ser. **384**, 012007 (2012) [arXiv:1201.4560 [astro-ph.CO]].
- [9] <http://www.nano-lab.com/alignedcarbonnanotubearrays.html>
- [10] S. Orlanducci, M.L. Terranova, *private communications*.
- [11] C. Laurent and E. Flahaut and A. Peigney, Carbon, **48** n.10 2994 (2010).
- [12] G. Alimonti *et al.* [Borexino Collaboration], Phys. Lett. B **422**, 349 (1998).